Journal of Applied Fluid Mechanics, Vol. 11, No. 3, pp. 597-612, 2018.
Available online at www.jafmonline.net, ISSN 1735-3572, EISSN 1735-3645.
DOI: 10.29252/jafm.11.03.27854

Ferrofluid Based Squeeze Film Lubrication between Rough Stepped Plates with Couple Stress Effect

Y. D. Vashi[1†], R. M. Patel[2] and G. M. Deheri[3]

[1] *Department of Applied Sciences and Humanity, Alpha College of Engineering and technology, Ahmedabad, Gujarat-382721, India.*
[2] *Department of Mathematics, Gujarat Arts and Science College, Ahmedabad, Gujarat-380006, India*
[3] *Department of Mathematics, Sardar Patel University, Vallabh Vidyanagar, Gujarat--388120, India*

†*Corresponding Author Email: yogini.vashi@gmail.com*

(Received April 9, 2017; accepted December 12, 2017)

ABSTRACT

This investigation purposes to study the magnetic fluid based squeeze film behavior on transversely rough stepped plates with the influence of couple stress. Using the well-known stochastic model of Christensen and Tonder the roughness effect has been evaluated. The magnetic fluid flow model of Neuringer - Roseinweig has been adopted to obtain the influence of magnetization. The governing Reynolds' type equation is derived on the basis of stokes microcontinum theory for couple stress fluid. For the expression of pressure distribution, the stochastically averaged Reynolds' type equation is solved. which results in calculation of load carrying capacity. The graphical outcomes also presented in tabular form suggest that although the bearing suffers on account of roughness, the magnetization and couple stress effect save the situation, as this combination does not allow the load carrying capacity to fall rapidly. However, in the case of negatively skewed roughness the magnetization goes a long way in dropping the adversarial influence of roughness by selecting an appropriate value of couple stress parameter when variance (-ve) is involved. It is found that the couple stress effect, alone may not be sufficient to counter the negative influence of transverse roughness and porosity. However, in almost all situations the ferrofluid lubrication adds significantly to the positive effect of couple stress to overcome the adversarial outcome of porosity and roughness. Further, the position of step plays a vital role for an all-round enhancement of the bearing performance.

Keywords: Squeeze film; Stepped plates; Roughness; Ferrofluid; Couple stress; Load carrying capacity.

NOMENCLATURE

b	width of the bearing	α	variance
H^*	non dimensional mean film thickness	α^*	non dimensional variance
H	thickness of the porous facing	ε	skewness
h_1	maximum film thickness	ε^*	non dimensional skewness
h_2	minimum film thickness	η	couple stress constant of the lubricant
KL	the position of the step $(0 < K < 1)$	l	couple stress parameter $\left(\sqrt{\frac{\eta}{\mu}}\right)$
L	length of the bearing	μ	viscosity of the lubricant
p_1	pressure in the fluid film region $(0 < x < KL)$	l^*	non dimensional couple stress parameter
p_2	pressure in the fluid film region $(KL < x < L)$	μ_0	permeability of the free space
P^*	pressure in the porous matrix	$\overline{\mu}$	magnetic susceptibility of particle
V	squeeze velocity	μ^*	non dimensional magnetization parameter
w	load carrying capacity	σ	standard deviation
$\overline{w}$	non dimensional load carrying capacity	$\overline{q}^*$	darcy velocity vector
		σ^*	non dimensional standard deviation

(u, v, w)	fluid velocity components
ϕ	permeability of the porous facing
$\bar{v}$	velocity vector
ψ	non dimensional porosity

1. INTRODUCTION

The squeeze film actions rise from the phenomena of two lubricated surfaces moving toward each other in the normal direction and produce a positive pressure and hence sustenance a load. The squeeze film lubrication can be found in bearings, machine tools, human body joins, rolling elements, IC engines and gears applications.

The study of non –Newtonian fluid dynamics is of vital importance in connection with plastic manufacturing, lubricating and movements of biological and geophysical fluids. The non-Newtonian behavior finds applications in the fields of rotating machinery, computer storage devices, viscometer, crystal growth processes and heat and mass transfer etc. (Hughes 1963, Bujurke 1987, Maiti 1973, Elkouh and Yang 1991). Stokes (1966) microcontinuum theory has been widely used to compute the influence of couple stresses on the performance of bearing systems by Ramanaiah and Dubey (1975). Now a days it is well known that the use of Newtonian fluids mixed with additives introduces a development in the bearing characteristics as compared to the Newtonian lubricants. In fact, due to the existence of additives a nonlinear relationship is create among the shear stress and strain rate. There are a number of fluid models considering the non-Newtonian properties of the lubricants such power law, couple stress and micro polar fluid. (Guha 2004, Ramanaiah and Sarkar 1978, Lin 1998). Lin *et al*. (2006) talked about averaged inertia principle for non-Newtonian squeeze films in wide parallel plates through couple stress fluid model. The load carrying capacity was observed to be increased because of the impact of couple stresses as compared to the Newtonian lubricant case.

Biradar (2013) investigated theoretically the influence of couple stress fluid on squeezing flow between porous parallel stepped plates. It was discovered that the due to the presence of couple stress effect in the lubricant the load bearing capacity got improved and reduced the response time as compared to Newtonian lubricant based bearing system.

The ferrofluid are colloidal suspensions composed of magnetic particles of subdomain size in a carrier. As is well known the key benefit of ferrofluid lubricants as a substitute of conventional one is that the former can be reserved at a desired position by an external magnetic field. Ferrofluids have been found to be used in many technological applications like dynamic sealing, heat dissipation, damping and medical applications like drug targeting, hyperthermia, cell separation etc. The brief study of above applications can be had from (Scherer and Figueiredo Neto, 2005). Huang and Wang (2016) prepared a review report on the progress of ferrofluid lubrication based on the three flow models of Neuringer–Rosensweig, Shliomis and Jenkins. They have briefly discussed some experimental studies on ferrofluid lubrication and concluded that over the conventional lubricant ferrofluid have considerably better friction decline and anti-wear abilities under the external magnetic field. Patel *et al*. (2017) examined experimentally the influence of ferrofluid based hydrodynamic journal bearing with different combination of materials.

Due to the random structure of surface roughness, a stochastic approach was employed to model the surface roughness (Christensen and Tonder 1969a, 1969b, 1970). The stochastic averaging method deployed in the above investigation found its applications in a number of investigations (Prakash and Tiwari 1983, Patel *et al*. 2008, Gupta and Deheri 1996). Patel *et al*. (2008, January) analyzed the performance of a squeeze film between infinitely long porous rough parallel plates with porous matrix of variable film thickness in the presence of a ferrofluid. The ferrofluid lubrication improved the bearing performance while, the composite roughness of the bearing surfaces induced an adversarial influence on the squeeze film behavior. Siddangouda (2015) studied the squeeze film characteristics between parallel stepped plates considering influence of couple stresses and surface roughness. It was noticed that the squeeze film characteristics got enhanced for transverse roughness whereas the bearing suffered owing to the existence of longitudinal roughness pattern. Vadher *et al*. (2008) considered the problem of squeeze films between electrically conducting rough porous surfaces and electrically conducting lubricant in the presence of a transverse roughness for a circular shape of the bearing surfaces. The negative influence of transverse surfaces roughness was reduced due to magnetization. This positive effect further enhanced in the case of negatively skewed roughness.

Patel and Deheri (2016) studied the influence of ferrofluid on rough parallel plate slider bearing. They have made a comparison between three ferrofluid flow models. Regarding the life period of bearing the Shliomis model is good for higher load while the Neuringer–Rosensweig model may be deployed for lower load. Shimpi and Deheri (2012) investigated the effect of deformation and surface roughness for ferrofluid based rotating porous curve circular plates. The load bearing capacity was found to be decreasing due to effect of rotation and deformation, it is improved due to ferrofluid lubrication in the case of negatively skewed roughness. The squeeze film characteristics for an infinitely long rough rectangular plate under the presence of a ferrofluid was examined by Deheri *et al*. (2006, September), this examination built up that the negative effect of surface roughness could be adjusted to a nominal extent by the ferrofluid lubrication.

So, the present study is made to observe the influence of a ferrofluid on squeeze film between rough stepped plates considering couple stress influence.

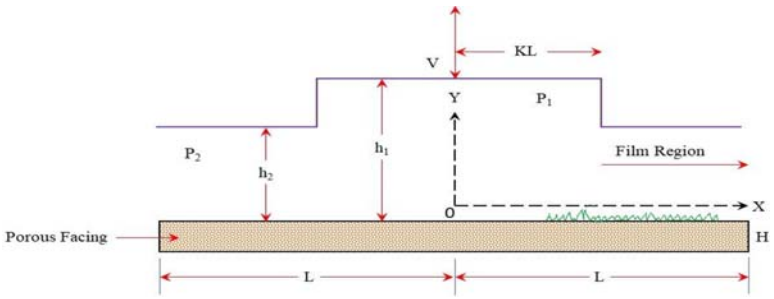

Fig. 1. Configuration of the bearing system.

2. ANALYSIS

Figure 1 indicates the structure of the bearing system where in, the squeeze film between parallel stepped plates moving toward each other with normal velocity V is depicted. All the principle of hydrodynamic lubrication is expected here. The lubricant is an incompressible Stoke couple stress fluid.

With the aid of Stokes (1966) microcontinum theory for couple stress fluid, following the study of Biradar (2012) the associated generalized Reyonlds' type equation for obtaining the pressure distribution is found to be

$$\frac{dp_i}{dx} = \frac{-12\,\mu Vx}{G_i(h_i, l)} \tag{1}$$

where,

$$G_i(h_i, l) = h^3 + 12\phi H - 12l^2 h + 24l^3 \tanh\left(\frac{h}{2l}\right)$$

for smooth bearing surfaces.

Now bring into the stochastic averaging techniques of Christensen and Tonder (19969a, 1969b, 1970) for transverse roughness one obtain the Reynolds' type equation governing the fluid film pressure

$$\frac{dp_i}{dx} = \frac{-12\,\mu Vx}{g_i(h_i, l)} \tag{2}$$

where,

$$g_i(h_i, l) = h^3 + 3\sigma^2 h + 3h^2\alpha + 3h\alpha^2 + 3\sigma^2\alpha + \alpha^3 + \varepsilon + 12\phi H - 12l^2 h + 24l^3 \tanh\left(\frac{h}{2l}\right)$$

Resorting to the magnetic fluid flow model of Neuringer Rosenweig (1964) the above Eq. (2) transforms to

$$\frac{d}{dx}\left[p_i - 0.5\mu_0 \bar{\mu} H^2\right] = \frac{-12\mu Vx}{g_i(h_i, l)} \tag{3}$$

where the magnitude of the magnetic field is described in the form of

$$H^2 = A(L - x)(x - KL)$$

where in A is a suitable constant dependent on the material to produce a field of desired magnetic strength.

Where,

$h_i = h_1$ for $0 \le x \le KL$ and

$h_i = h_2$ for $KL \le x \le L$

The associated boundary conditions are

$$p_1 = p_2 \text{ at } x = KL \text{ and } p_2 = 0 \text{ at } x = L \tag{4}$$

The solution of Eq. (3) under the above boundary condition is given respectively, by

$$p_1 = \frac{6\mu V}{g_1(h_1, l)}\left(K^2L^2 - x^2\right) + \frac{6\mu V}{g_2(h_2, l)}\left(L^2 - K^2L^2\right) + 0.5\mu_0\bar{\mu}H^2 \tag{5}$$

$$p_2 = \frac{6\mu V}{g_2(h_2, l)}\left(L^2 - x^2\right) + 0.5\mu_0\bar{\mu}H^2 \tag{6}$$

The load bearing capacity w is obtained as

$$w = 2b\int_0^{KL} p_1 dx + 2b\int_{KL}^{L} p_2 dx \tag{7}$$

which takes the form

$$w = \frac{bL^3 A\mu_0\bar{\mu}}{6}(1 - 3K) + 8b\mu VL^3\left[\frac{K^3}{g_1(h_1, l)} + \frac{\left(1 - K^3\right)}{g_2(h_2, l)}\right] \tag{8}$$

Then the load carrying capacity can be described in dimensionless form as

$$\bar{w} = \frac{wh_2^3}{8\mu VbL^3} = \frac{\mu^*(3K - 1)}{6} + 8b\mu VL^3\left[\frac{K^3}{g_1(H^*, l^*)} + \frac{\left(1 - K^3\right)}{g_2(1, l^*)}\right] \tag{9}$$

where

$$\mu^* = -\frac{\mu_0 \bar{\mu} A h_2^3}{8\mu V}$$

$$g_1\left(H^*, l^*\right) = H^{*3} + 3\sigma^{*2} H^* + 3H^{*2}\alpha^* + 3H^*\alpha^{*2} + 3\sigma^{*2}\alpha^* + \alpha^{*3} + \varepsilon^* + 12\psi - 3l^{*2} H^* + 3l^{*3} \tanh\left(\frac{H^*}{l^*}\right)$$

$$g_2\left(1, l^*\right) = 1 + 3\sigma^{*2} + 3\alpha^* + 3\alpha^{*2} + 3\sigma^{*2}\alpha^* + \alpha^{*3} + \varepsilon^* + 12\psi - 3l^{*2} + 3l^{*3} \tanh\left(\frac{1}{l^*}\right)$$

where

$$H^* = \frac{h_1}{h_2}, l^* = \frac{2l}{h_2}, \alpha^* = \frac{\alpha}{h_2},$$

$$\varepsilon^* = \frac{\varepsilon}{h_2^3}, \sigma^* = \frac{\sigma}{h_2}, \psi = \frac{\phi H}{h_2^3}$$

3. RESULT AND DISCUSSION

The Eq. (9) resolute the non-dimensional load carrying capacity. This equation suggests that the load bearing capacity improve by $\frac{\mu^*(3K-1)}{6}$, as compared to the case of couple stress fluid based bearing system. As the expression in the Eq. (9) is linear concerned with μ^* it is easy to see that an increase in the value μ^* of would lead to improved load carrying capacity. The magnetization boosts the viscosity of the fluid resulting in increased pressure and hence the load carrying capacity. The profile of load carrying capacity concerned with magnetization parameter existing in Figs. 2-8 makes it clear that the load carrying capacity increases with regards to magnetization. However, the influence of variance accompanying with roughness on the distribution of load bearing capacity with regards to μ^* remains negligible. Further, the skewness introduces a minimal effect on the load profile due to magnetization. In addition, the influence of porosity on variation of load bearing capacity with regards to μ^* is almost negligible up to the porosity value 0.01.

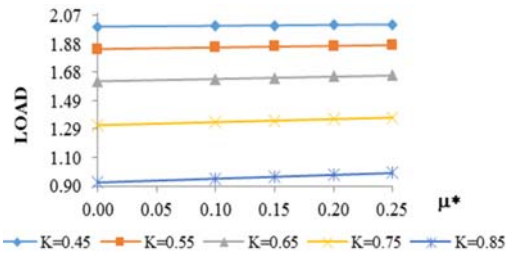

Fig. 2. Variation of $\bar{w}$ for the combination of μ^* and K.

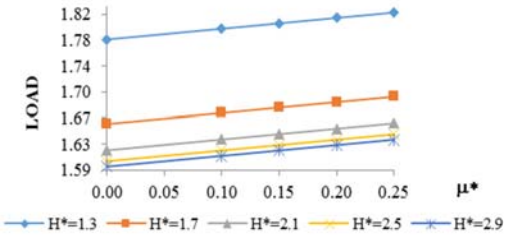

Fig. 3. Distribution of $\bar{w}$ with regards to μ^* and H^*.

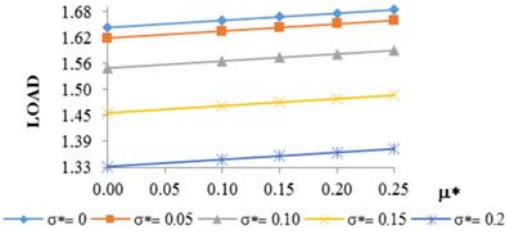

Fig. 4. Profile of $\bar{w}$ with reference to μ^* and σ^*.

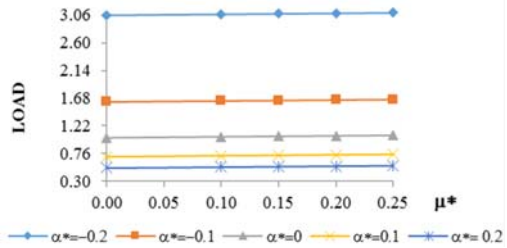

Fig. 5. Change in $\bar{w}$ concerned with μ^* and α^*.

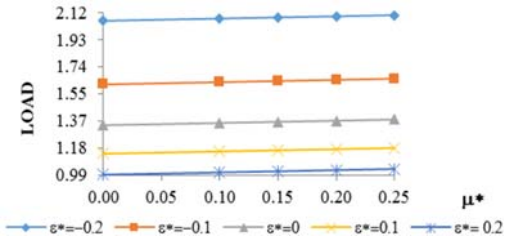

Fig. 6. Trends of $\bar{w}$ with regards to μ^* and ε^*.

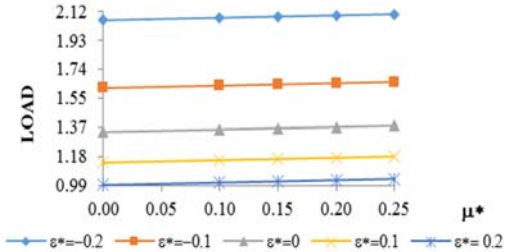

Fig. 7. Variation of $\bar{w}$ concerned with μ^* and ψ.

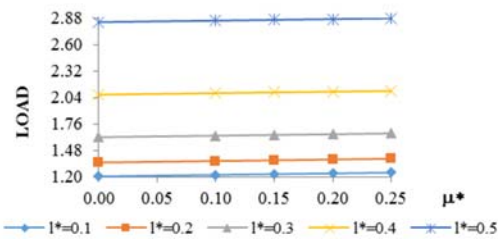

Fig. 8. Distribution of $\overline{w}$ reference to μ^* and l^*.

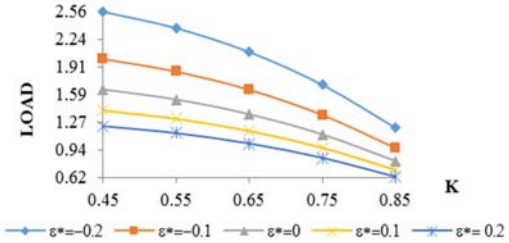

Fig. 12. Variation of $\overline{w}$ with reference to K and ε^*.

Figures 9-14 describe the trends of load bearing capacity with regards to step location. This graphs underline that the step location has a prominent role for improving the bearing characteristics. It is observed from Fig. 13 that the influence of porosity on the load bearing capacity concerned with step location is almost negligible, up to the porosity value 0.01. It is seen that the load bearing capacity drops with the increase in step location. Besides, bearing load reduction is observed due to roughness.

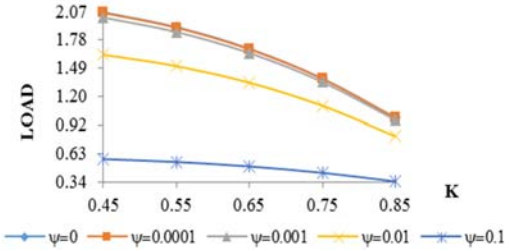

Fig. 13. Distribution of $\overline{w}$ for the combination of K and ψ.

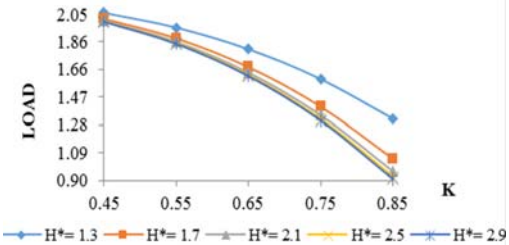

Fig. 9. Profile of $\overline{w}$ for the combination of K and H^*.

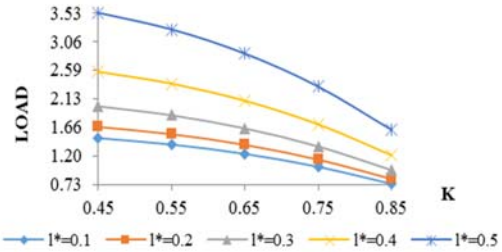

Fig. 14. Profile of $\overline{w}$ with regards to K and l^*.

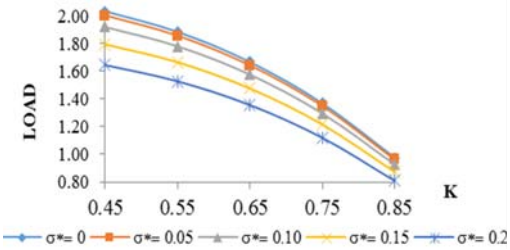

Fig. 10. Change in $\overline{w}$ with regards to K and σ^*.

The influence of film thickness ratio H^* on the variation of load carrying capacity is presented in Figs. 15-19. It is observed that initially there is a sharp decline in the load bearing capacity. Further, it is observed that the influence of roughness parameters and porosity on the variation of load carrying capacity with regards to film thickness ratio remains negligible when the film thickness ratio exceeds the value 2.5. However, the effect of couple stress remains visibly distinct.

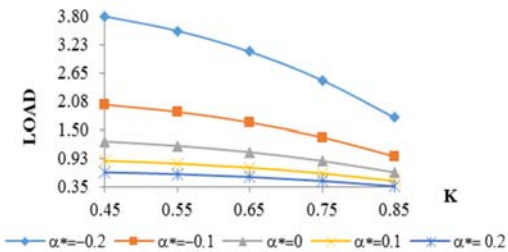

Fig. 11. Trends of $\overline{w}$ concerned with K and α^*.

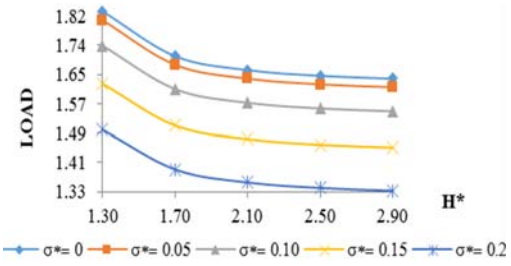

Fig. 15. Change in $\overline{w}$ concerned with H^* and σ^*.

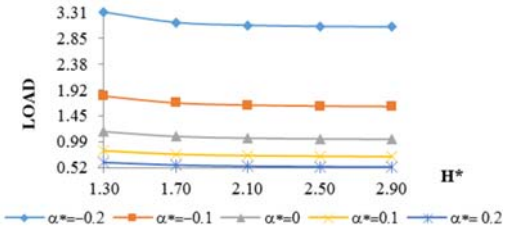

Fig. 16. Trends of $\overline{w}$ reference to H^* and α^*.

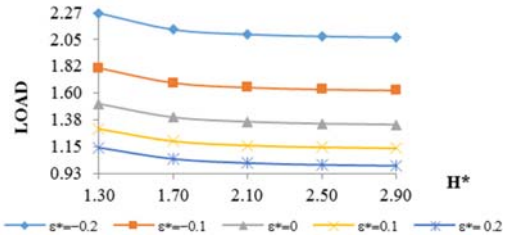

Fig. 17. Variation of $\overline{w}$ for the combination of H^* and ε^*.

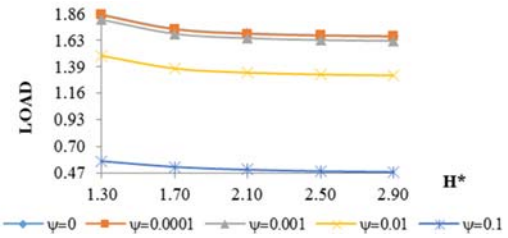

Fig. 18. Distribution of $\overline{w}$ with regards to H^* and ψ.

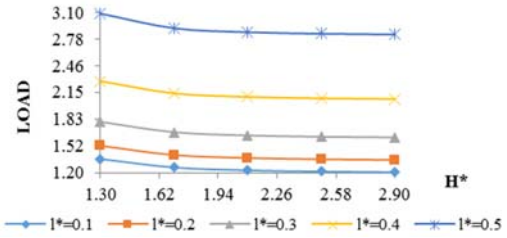

Fig. 19. Profile of $\overline{w}$ concerned with H^* and l^*.

The influence of standard deviation shown in Figs. 20-23 advises that there is considerable decrease in load carrying capacity, however the case of porosity where the effect is negligible up to 0.01. Thus, the trio of porosity, roughness and step location considerably influence the performance characteristics. The roughness of the bearing surfaces opposes the motion of the lubricant culminating in decreases pressure and hence the load bearing capacity.

The load carrying capacity gets reduced owing to positive variance, while the load carrying capacity gets increased with variance (-ve) (Figs. 24-26). Therefore, the positive effect of negatively skewed roughness and variance (-ve) may be duly considered while designing the bearing system.

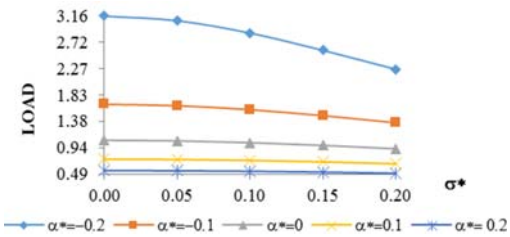

Fig. 20. Change in $\overline{w}$ reference to σ^* and α^*.

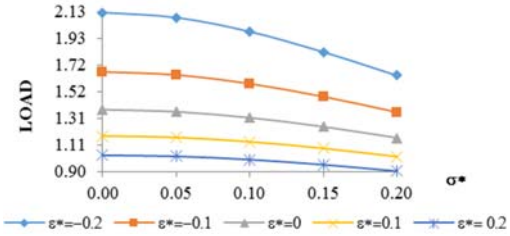

Fig. 21. Trends of $\overline{w}$ for the combination of σ^* and ε^*.

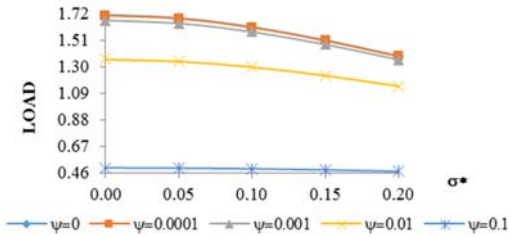

Fig. 22. Variation of $\overline{w}$ with regards to σ^* and ψ.

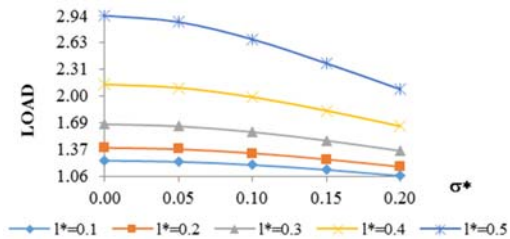

Fig. 23. Distribution of $\overline{w}$ concerned with σ^* and l^*.

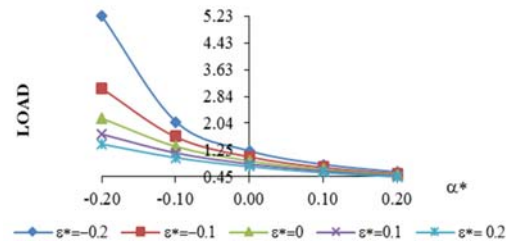

Fig. 24. Profile of $\overline{w}$ reference to α^* and ε^*.

Table 1 Variation of $\bar{w}$ for the combination of μ^* and K

$H^* = 2.10, \sigma^* = 0.05, \alpha^* = -0.10, \varepsilon^* = -0.10, l^* = 0.30, \psi = 0.001$					
	$K = 0.45$	$K = 0.55$	$K = 0.65$	$K = 0.75$	$K = 0.85$
$\mu^* = 0$	1.99433489	1.84034142	1.61881593	1.31747988	0.92405471
$\mu^* = 0.1$	2.00016822	1.85117475	1.63464927	1.33831321	0.94988805
$\mu^* = 0.15$	2.00308489	1.85659142	1.64256593	1.34872988	0.96280471
$\mu^* = 0.20$	2.00600155	1.86200809	1.65048260	1.35914655	0.97572138
$\mu^* = 0.25$	2.00891822	1.86742475	1.65839927	1.36956321	0.98863805

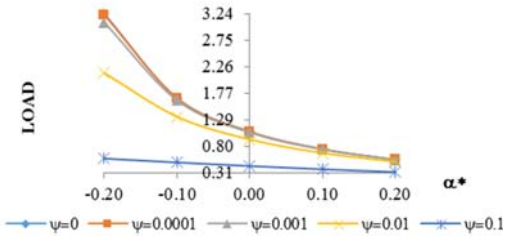

Fig. 25. Change in $\bar{w}$ for the combination of α^* and ψ.

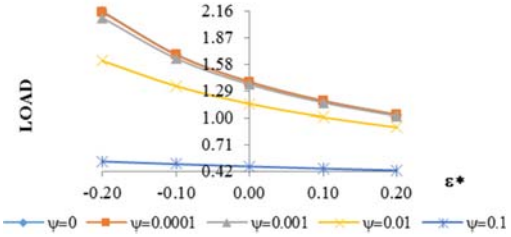

Fig. 27. Variation of $\bar{w}$ concerned with ε^* and ψ.

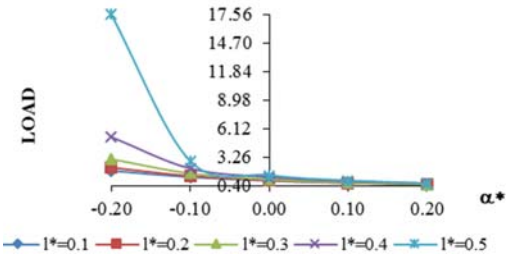

Fig. 26. Trends of $\bar{w}$ with regards to α^* and l^*.

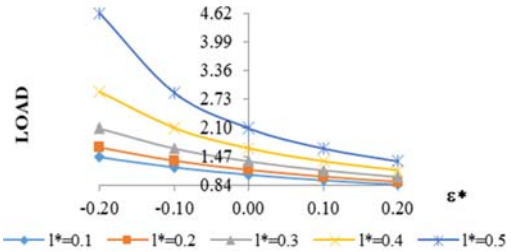

Fig. 28. Distribution of $\bar{w}$ with reference to ε^* and l^*.

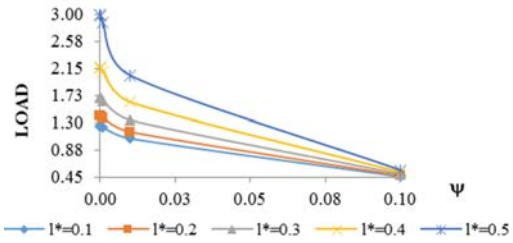

Fig. 29. Profile of $\bar{w}$ for the combination of ψ and l^*.

From Fig. 29 and some of the earlier graphs one can easily accomplish that the porosity effect is at the best nominal. However, the positive effect of couple stress is manifest as can be seen from Figs. 19, 23, 26, 28, 29. Indeed, the presence of micro structure additive in the lubricant gives rise to an increase in squeeze film pressure and therefore the load carrying capacity. The couple stress parameter delivers a mechanism for the interface of the lubricant with bearing geometry.

Some of the graphical representations make it sure, that the affirmative influence of magnetic fluid lubrication under the couple stress effect may be sufficient to overcome the adversarial effect of roughness and porosity, for a suitable choice of step location. Now a days ferrofluid are available easily and therefore ferrofluid lubrication of this type of bearing system will be favorable to the industry for

Table 2 Distribution of $\overline{w}$ with regards to μ^* and H^*

$K = 0.65, \sigma^* = 0.05, \alpha^* = -0.10, \varepsilon^* = -0.10, l^* = 0.30, \psi = 0.001$					
	$H^* = 1.3$	$H^* = 1.7$	$H^* = 2.1$	$H^* = 2.5$	$H^* = 2.9$
$\mu^* = 0$	1.78106089	1.65731397	1.61881593	1.60277709	1.59487334
$\mu^* = 0.1$	1.79689423	1.67314730	1.63464927	1.61861043	1.61070667
$\mu^* = 0.15$	1.80481089	1.68106397	1.64256593	1.62652709	1.61862334
$\mu^* = 0.20$	1.81272756	1.68898064	1.65048260	1.63444376	1.62654000
$\mu^* = 0.25$	1.82064423	1.69689730	1.65839927	1.64236043	1.63445667

Table 3 Profile of $\overline{w}$ with reference to μ^* and σ^*

$H^* = 2.10, K = 0.65, \alpha^* = -0.10, \varepsilon^* = -0.10, l^* = 0.30, \psi = 0.001$					
	$\sigma^* = 0$	$\sigma^* = 0.05$	$\sigma^* = 0.10$	$\sigma^* = 0.15$	$\sigma^* = 0.20$
$\mu^* = 0$	1.64252489	1.61881593	1.55168921	1.45156534	1.33161271
$\mu^* = 0.1$	1.65835822	1.63464927	1.56752254	1.46739867	1.34744605
$\mu^* = 0.15$	1.66627489	1.64256593	1.57543921	1.47531534	1.35536271
$\mu^* = 0.20$	1.67419156	1.65048260	1.58335588	1.48323201	1.36327938
$\mu^* = 0.25$	1.68210822	1.65839927	1.59127254	1.49114867	1.37119605

Table 4 Change in $\overline{w}$ concerned with μ^* and α^*

$H^* = 2.10, \sigma^* = 0.05, K = 0.65, \varepsilon^* = -0.10, l^* = 0.30, \psi = 0.001$					
	$\alpha^* = -0.2$	$\alpha^* = -0.1$	$\alpha^* = 0$	$\alpha^* = 0.1$	$\alpha^* = 0.2$
$\mu^* = 0$	3.05602498	1.61881593	1.02482034	0.71021514	0.52055594
$\mu^* = 0.1$	3.07185831	1.63464927	1.04065368	0.72604848	0.53638927
$\mu^* = 0.15$	3.07977498	1.64256593	1.04857034	0.73396514	0.54430594
$\mu^* = 0.20$	3.08769165	1.65048260	1.05648701	0.74188181	0.55222261
$\mu^* = 0.25$	3.09560831	1.65839927	1.06440368	0.74979848	0.56013927

Table 5 Trends of $\overline{w}$ with regards to μ^* and ε^*

$H^* = 2.10, \sigma^* = 0.05, \alpha^* = -0.10, K = 0.65, l^* = 0.30, \psi = 0.001$					
	$\varepsilon^* = -0.2$	$\varepsilon^* = -0.1$	$\varepsilon^* = 0$	$\varepsilon^* = 0.1$	$\varepsilon^* = 0.2$
$\mu^* = 0$	2.06052214	1.61881593	1.33510645	1.13742379	0.99174937
$\mu^* = 0.1$	2.07635547	1.63464927	1.35093979	1.15325712	1.00758270
$\mu^* = 0.15$	2.08427214	1.64256593	1.35885645	1.16117379	1.01549937
$\mu^* = 0.20$	2.09218881	1.65048260	1.36677312	1.16909045	1.02341604
$\mu^* = 0.25$	2.10010547	1.65839927	1.37468979	1.17700712	1.03133270

Table 6 Variation of $\overline{w}$ concerned with μ^* and ψ

$H^* = 2.10, \sigma^* = 0.05, \alpha^* = -0.10, \varepsilon^* = -0.10, l^* = 0.30, K = 0.65$					
	$\psi = 0$	$\psi = 0.0001$	$\psi = 0.001$	$\psi = 0.01$	$\psi = 0.1$
$\mu^* = 0$	1.66138626	1.65702668	1.61881593	1.31672946	0.47236975
$\mu^* = 0.1$	1.67721959	1.67286001	1.63464927	1.33256280	0.48820308
$\mu^* = 0.15$	1.68513626	1.68077668	1.64256593	1.34047946	0.49611975
$\mu^* = 0.20$	1.69305293	1.68869335	1.65048260	1.34839613	0.50403641
$\mu^* = 0.25$	1.70096959	1.69661001	1.65839927	1.35631280	0.51195308

Table 7 Distribution of $\overline{w}$ reference to μ^* and l^*

$H^* = 2.10, K = 0.65, \sigma^* = 0.05, \alpha^* = -0.10, \varepsilon^* = -0.10, \psi = 0.001$					
	$l^* = 0.1$	$l^* = 0.2$	$l^* = 0.3$	$l^* = 0.4$	$l^* = 0.5$
$\mu^* = 0$	1.20345459	1.35035597	1.61881593	2.06945891	2.83868862
$\mu^* = 0.1$	1.21928793	1.36618930	1.63464927	2.08529224	2.85452196
$\mu^* = 0.15$	1.22720459	1.37410597	1.64256593	2.09320891	2.86243862
$\mu^* = 0.20$	1.23512126	1.38202264	1.65048260	2.10112557	2.87035529
$\mu^* = 0.25$	1.24303793	1.38993930	1.65839927	2.10904224	2.87827196

Table 8 Profile of $\overline{w}$ for the combination of K and H^*

$\mu^* = 0.15, \sigma^* = 0.05, \alpha^* = -0.10, \varepsilon^* = -0.10, l^* = 0.30, \psi = 0.001$					
	$H^* = 1.3$	$H^* = 1.7$	$H^* = 2.1$	$H^* = 2.5$	$H^* = 2.9$
$K = 0.45$	2.05692038	2.01585915	2.00308489	1.99776294	1.99514035
$K = 0.55$	1.95488365	1.87991453	1.85659142	1.84687467	1.84208637
$K = 0.65$	1.80481089	1.68106397	1.64256593	1.62652709	1.61862334
$K = 0.75$	1.59796827	1.40787001	1.34872988	1.32409124	1.31194961
$K = 0.85$	1.32562196	1.04889522	0.96280471	0.92693816	0.90926353

Table 9 Change in $\overline{w}$ with regards to K and σ^*

$\mu^* = 0.15, H^* = 2.10, \alpha^* = -0.10, \varepsilon^* = -0.10, l^* = 0.30, \psi = 0.001$					
	$\sigma^* = 0$	$\sigma^* = 0.05$	$\sigma^* = 0.10$	$\sigma^* = 0.15$	$\sigma^* = 0.20$
$K = 0.45$	2.03272289	2.00308489	1.91918130	1.79406404	1.64422495
$K = 0.55$	1.88379803	1.85659142	1.77956772	1.66469979	1.52711659
$K = 0.65$	1.66627489	1.64256593	1.57543921	1.47531534	1.35536271
$K = 0.75$	1.36768106	1.34872988	1.29506579	1.21499792	1.11902776
$K = 0.85$	0.97554413	0.96280471	0.92671746	0.87283478	0.80817618

Table 10 Trends of $\bar{w}$ concerned with K and α^*

$\mu^* = 0.15, H^* = 2.10, \sigma^* = 0.05, \varepsilon^* = -0.10, l^* = 0.30, \psi = 0.001$					
	$\alpha^* = -0.2$	$\alpha^* = -0.1$	$\alpha^* = 0$	$\alpha^* = 0.1$	$\alpha^* = 0.2$
$K = 0.45$	3.79770640	2.00308489	1.26375369	0.87355974	0.63920360
$K = 0.55$	3.50464461	1.85659142	1.17685970	0.81766332	0.60163657
$K = 0.65$	3.07977498	1.64256593	1.04857034	0.73396514	0.54430594
$K = 0.75$	2.49913246	1.34872988	0.87135919	0.61741035	0.46361831
$K = 0.85$	1.73875199	0.96280471	0.63769980	0.46294407	0.35598030

Table 11 Variation of $\bar{w}$ with reference to K and ε^*

$\mu^* = 0.15, H^* = 2.10, \sigma^* = 0.05, \alpha^* = -0.10, l^* = 0.30, \psi = 0.001$					
	$\varepsilon^* = -0.2$	$\varepsilon^* = -0.1$	$\varepsilon^* = 0$	$\varepsilon^* = 0.1$	$\varepsilon^* = 0.2$
$K = 0.45$	2.55606755	2.00308489	1.64805551	1.40080357	1.21870521
$K = 0.55$	2.36394164	1.85659142	1.53080903	1.30388455	1.13672298
$K = 0.65$	2.08427214	1.64256593	1.35885645	1.16117379	1.01549937
$K = 0.75$	1.70114204	1.34872988	1.12225122	0.96434552	0.84789959
$K = 0.85$	1.19863432	0.96280471	0.81104675	0.70507399	0.62678884

Table 12 Distribution of $\bar{w}$ for the combination of K and ψ

$H^* = 2.10, \sigma^* = 0.05, \alpha^* = -0.10, \varepsilon^* = -0.10, l^* = 0.30, \mu^* = 0.15$					
	$\psi = 0$	$\psi = 0.0001$	$\psi = 0.001$	$\psi = 0.01$	$\psi = 0.1$
$K = 0.45$	2.05636942	2.05091249	2.00308489	1.62506520	0.57129979
$K = 0.55$	1.90548225	1.90047532	1.85659142	1.50971056	0.54181860
$K = 0.65$	1.68513626	1.68077668	1.64256593	1.34047946	0.49611975
$K = 0.75$	1.38270257	1.37922356	1.34872988	1.10757620	0.43125456
$K = 0.85$	0.98555229	0.98322296	0.96280471	0.80120504	0.34427438

Table 13 Profile of $\bar{w}$ with regards to K and l^*

$\mu^* = 0.15, H^* = 2.10, \sigma^* = 0.05, \alpha^* = -0.10, \varepsilon^* = -0.10, \psi = 0.001$					
	$l^* = 0.1$	$l^* = 0.2$	$l^* = 0.3$	$l^* = 0.4$	$l^* = 0.5$
$K = 0.45$	1.48448946	1.66785118	2.00308489	2.56615043	3.52794256
$K = 0.55$	1.38033041	1.54874041	1.85659142	2.37355452	3.25638032
$K = 0.65$	1.22720459	1.37410597	1.64256593	2.09320891	2.86243862
$K = 0.75$	1.01620897	1.13385266	1.34872988	1.70915910	2.32386666
$K = 0.85$	0.73844049	0.81788527	0.96280471	1.20545062	1.61841362

Table 14 Change in $\bar{w}$ concerned with H^* and σ^*

$K = 0.65, \psi = 0.001, \alpha^* = -0.10, \varepsilon^* = -0.10, l^* = 0.30, \mu^* = 0.15$					
	σ*= 0̃	σ*= 0.05	σ*= 0.10	σ*= 0.15	σ*= 0.2
$H^* = 1.3$	1.82975362	1.80481089	1.73408155	1.62826375	1.50093264
$H^* = 1.7$	1.70494765	1.68106397	1.61342104	1.51246256	1.39139272
$H^* = 2.1$	1.66627489	1.64256593	1.57543921	1.47531534	1.35536271
$H^* = 2.5$	1.65019008	1.62652709	1.55953695	1.45963637	1.33998757
$H^* = 2.9$	1.64227061	1.61862334	1.55168003	1.45185648	1.33231339

Table 15 Trends of $\bar{w}$ reference to H^* and α^*

$\mu^* = 0.15, K = 0.65, l^* = 0.3, \sigma^* = 0.05, \varepsilon^* = -0.10, \psi = 0.001$					
	$\alpha^* = -0.2$	$\alpha^* = -0.1$	$\alpha^* = 0$	$\alpha^* = 0.1$	$\alpha^* = 0.2$
$H^* = 1.3$	3.31605909	1.80481089	1.16556278	0.82134448	0.61134080
$H^* = 1.7$	3.13022019	1.68106397	1.07859282	0.75779925	0.56351389
$H^* = 2.1$	3.07977498	1.64256593	1.04857034	0.73396514	0.54430594
$H^* = 2.5$	3.06005428	1.62652709	1.03536937	0.72298598	0.53509007
$H^* = 2.9$	3.05069876	1.61862334	1.02864066	0.71721783	0.53011419

Table 16 Variation of $\bar{w}$ for the combination of H^* and ε^*

$\mu^* = 0.15, K = 0.65, l^* = 0.3, \sigma^* = 0.05, \alpha^* = -0.10, \psi = 0.001$					
	$\varepsilon^* = -0.2$	$\varepsilon^* = -0.1$	$\varepsilon^* = 0$	$\varepsilon^* = 0.1$	$\varepsilon^* = 0.2$
$H^* = 1.3$	2.26158560	1.80481089	1.50812527	1.29915925	1.14359003
$H^* = 1.7$	2.12439631	1.68106397	1.39582881	1.19671254	1.04968913
$H^* = 2.1$	2.08427214	1.64256593	1.35885645	1.16117379	1.01549937
$H^* = 2.5$	2.06789033	1.62652709	1.34314965	1.14578857	1.00042573
$H^* = 2.9$	2.05988828	1.61862334	1.33534236	1.13807596	0.99280605

Table 17 Distribution of $\bar{w}$ with regards to H^* and ψ

$\mu^* = 0.15, K = 0.65, l^* = 0.3, \sigma^* = 0.05, \alpha^* = -0.10, \varepsilon^* = -0.10$					
	$\psi = 0$	$\psi = 0.0001$	$\psi = 0.001$	$\psi = 0.01$	$\psi = 0.1$
$H^* = 1.3$	1.84906987	1.84454005	1.80481089	1.48878786	0.57127795
$H^* = 1.7$	1.72382395	1.71944534	1.68106397	1.37733384	0.52115213
$H^* = 2.1$	1.68513626	1.68077668	1.64256593	1.34047946	0.49611975
$H^* = 2.5$	1.66905685	1.66470133	1.62652709	1.32479877	0.48343422
$H^* = 2.9$	1.66114140	1.65678705	1.61862334	1.31699911	0.47656986

Table 18 Profile of $\bar{w}$ concerned with H^* and l^*

$\mu^* = 0.15, K = 0.65, \psi = 0.001, \sigma^* = 0.05, \alpha^* = -0.10, \varepsilon^* = -0.10$					
	$l^* = 0.1$	$l^* = 0.2$	$l^* = 0.3$	$l^* = 0.4$	$l^* = 0.5$
$H^* = 1.3$	1.36255340	1.51946741	1.80481089	2.28035340	3.08444121
$H^* = 1.7$	1.26143635	1.40995268	1.68106397	2.13545816	2.90965769
$H^* = 2.1$	1.22720459	1.37410597	1.64256593	2.09320891	2.86243862
$H^* = 2.5$	1.21236811	1.35881155	1.62652709	2.07613508	2.84402442
$H^* = 2.9$	1.20489301	1.35117287	1.61862334	2.06786563	2.83528645

Table 19 Change in $\bar{w}$ reference to σ^* and α^*

$\mu^* = 0.15, K = 0.65, \psi = 0.001, l^* = 0.3, H^* = 2.10, \varepsilon^* = -0.10$					
	$\alpha^* = -0.2$	$\alpha^* = -0.1$	$\alpha^* = 0$	$\alpha^* = 0.1$	$\alpha^* = 0.2$
$\sigma^* = 0$	3.15685434	1.66627489	1.05893406	0.73935682	0.54742367
$\sigma^* = 0.05$	3.07977498	1.64256593	1.04857034	0.73396514	0.54430594
$\sigma^* = 0.10$	2.86995657	1.57543921	1.01871261	0.71827807	0.53517729
$\sigma^* = 0.15$	2.57830914	1.47531534	0.97271027	0.69365257	0.52067184
$\sigma^* = 0.20$	2.25874502	1.35536271	0.91515090	0.66203549	0.50172729

Table 20 Trends of $\bar{w}$ for the combination of σ^* and ε^*

$\mu^* = 0.15, K = 0.65, \psi = 0.001, l^* = 0.3, H^* = 2.10, \alpha^* = -0.10$					
	$\varepsilon^* = -0.2$	$\varepsilon^* = -0.1$	$\varepsilon^* = 0$	$\varepsilon^* = 0.1$	$\varepsilon^* = 0.2$
$\sigma^* = 0$	2.12316692	1.66627489	1.37481567	1.17265147	1.02415416
$\sigma^* = 0.05$	2.08427214	1.64256593	1.35885645	1.16117379	1.01549937
$\sigma^* = 0.10$	1.97589040	1.57543921	1.31320380	1.12810358	0.99042958
$\sigma^* = 0.15$	1.81885496	1.47531534	1.24379761	1.07714243	0.95140591
$\sigma^* = 0.20$	1.63765559	1.35536271	1.15850849	1.01336236	0.90188594

Table 21 Variation of $\bar{w}$ with regards to σ^* and ψ

$\mu^* = 0.15, K = 0.65, l^* = 0.3, H^* = 2.10, \alpha^* = -0.10, \varepsilon^* = -0.10$					
	$\psi = 0$	$\psi = 0.0001$	$\psi = 0.001$	. $\psi = 0.01$	$\psi = 0.1$
$\sigma^* = 0$	1.71014279	1.70564871	1.66627489	1.35599037	0.49798861
$\sigma^* = 0.05$	1.68513626	1.68077668	1.64256593	1.34047946	0.49611975
$\sigma^* = 0.10$	1.61444472	1.61045428	1.57543921	1.29607957	0.49060244
$\sigma^* = 0.15$	1.50930201	1.50583031	1.47531534	1.22849361	0.48169396
$\sigma^* = 0.20$	1.38380448	1.38090446	1.35536271	1.14530162	0.46979020

Table 22 Distribution of $\bar{w}$ concerned with σ^* and l^*

$\mu^* = 0.15, K = 0.65, \psi = 0.001, H^* = 2.10, \alpha^* = -0.10, \varepsilon^* = -0.10$					
	$l^* = 0.1$	$l^* = 0.2$	$l^* = 0.3$	$l^* = 0.4$	$l^* = 0.5$
$\sigma^* = 0$	1.24011767	1.39045847	1.66627489	2.13240867	2.93732116
$\sigma^* = 0.05$	1.22720459	1.37410597	1.64256593	2.09320891	2.86243862
$\sigma^* = 0.10$	1.19009020	1.32735588	1.57543921	1.98400678	2.65946738
$\sigma^* = 0.15$	1.13316179	1.25635955	1.47531534	1.82585920	2.37942580
$\sigma^* = 0.20$	1.06236236	1.16924569	1.35536271	1.64348814	2.07533218

Table 23 Profile of $\bar{w}$ reference to α^* and ε^*

$\mu^* = 0.15, K = 0.65, l^* = 0.3, H^* = 2.10, \sigma^* = 0.05, \psi = 0.001$					
	$\varepsilon^* = -0.2$	$\varepsilon^* = -0.1$	$\varepsilon^* = 0$	$\varepsilon^* = 0.1$	$\varepsilon^* = 0.2$
$\alpha^* = -0.2$	5.22007685	3.07977498	2.19514983	1.71161449	1.40667915
$\alpha^* = -0.1$	2.08427214	1.64256593	1.35885645	1.16117379	1.01549937
$\alpha^* = 0$	1.20652458	1.04857034	0.92858386	0.83432375	0.75830112
$\alpha^* = 0.1$	0.80523212	0.73396514	0.67492242	0.62519925	0.58274392
$\alpha^* = 0.2$	0.58105390	0.54430594	0.51224703	0.48403021	0.45900098

Table 24 Change in $\bar{w}$ for the combination of α^* and ψ

$\mu^* = 0.15, K = 0.65, l^* = 0.3, H^* = 2.10, \sigma^* = 0.05, \varepsilon^* = -0.10$					
	$\psi = 0$	$\psi = 0.0001$	$\psi = 0.001$	$\psi = 0.01$	$\psi = 0.1$
$\alpha^* = -0.2$	3.23785677	3.22130665	3.07977498	2.14627697	0.56811239
$\alpha^* = -0.1$	1.68513626	1.68077668	1.64256593	1.34047946	0.49611975
$\alpha^* = 0$	1.06520764	1.06351899	1.04857034	0.92021826	0.42965129
$\alpha^* = 0.1$	0.74180292	0.74101112	0.73396514	0.67063325	0.37048200
$\alpha^* = 0.2$	0.54844897	0.54803160	0.54430594	0.50985803	0.31916247

Table 25 Trends of $\bar{w}$ with regards to α^* and l^*

$\mu^* = 0.15, K = 0.65, \psi = 0.001, H^* = 2.10, \sigma^* = 0.05, \varepsilon^* = -0.10$					
	$l^* = 0.1$	$l^* = 0.2$	$l^* = 0.3$	$l^* = 0.4$	$l^* = 0.5$
$\alpha^* = -0.2$	1.86452288	2.23742673	3.07977498	5.27219007	17.54748187
$\alpha^* = -0.1$	1.22720459	1.37410597	1.64256593	2.09320891	2.86243862
$\alpha^* = 0$	0.86657863	0.93524384	1.04857034	1.20989775	1.42415520
$\alpha^* = 0.1$	0.64236934	0.67818324	0.73396514	0.80695056	0.89379989
$\alpha^* = 0.2$	0.49377673	0.51396997	0.54430594	0.58207610	0.62441538

Table 26 Variation of $\bar{w}$ concerned with ε^* and ψ

$\mu^* = 0.15, K = 0.65, H^* = 2.10, \sigma^* = 0.05, \alpha^* = -0.10, l^* = 0.3$					
	$\psi = 0$	$\psi = 0.0001$	$\psi = 0.001$	$\psi = 0.01$	$\psi = 0.1$
$\varepsilon^* = -0.2$	2.15438897	2.14715971	2.08427214	1.61540073	0.52497860
$\varepsilon^* = -0.1$	1.68513626	1.68077668	1.64256593	1.34047946	0.49611975
$\varepsilon^* = 0$	1.38742870	1.38451524	1.35885645	1.14791597	0.47053140
$\varepsilon^* = 0.1$	1.18167408	1.17958996	1.16117379	1.00548265	0.44768330
$\varepsilon^* = 0.2$	1.03092564	1.02936081	1.01549937	0.89582808	0.42715413

Table 27 Distribution of $\bar{w}$ with reference to ε^* and l^*

$\mu^* = 0.15, K = 0.65, \psi = 0.001, H^* = 2.10, \sigma^* = 0.05, \alpha^* = -0.10$					
	$l^* = 0.1$	$l^* = 0.2$	$l^* = 0.3$	$l^* = 0.4$	$l^* = 0.5$
$\varepsilon^* = -0.2$	1.45205080	1.66559742	2.08427214	2.88341662	4.61984063
$\varepsilon^* = -0.1$	1.22720459	1.37410597	1.64256593	2.09320891	2.86243862
$\varepsilon^* = 0$	1.06463724	1.17193166	1.35885645	1.64846332	2.08305626
$\varepsilon^* = 0.1$	0.94158832	1.02343505	1.16117379	1.36318178	1.64283839
$\varepsilon^* = 0.2$	0.84518503	0.90971359	1.01549937	1.16457568	1.35985797

Table 28 Profile of $\bar{w}$ for the combination of ψ and l^*

$\mu^* = 0.15, K = 0.65, \alpha^* = -0.10, H^* = 2.10, \sigma^* = 0.05, \varepsilon^* = -0.10$					
	$l^* = 0.1$	$l^* = 0.2$	$l^* = 0.3$	$l^* = 0.4$	$l^* = 0.5$
$\psi = 0$	1.25029292	1.40339054	1.68513626	2.16387525	2.99829704
$\psi = 0.0001$	1.24794329	1.40040372	1.68077668	2.15658847	2.98412096
$\psi = 0.001$	1.22720459	1.37410597	1.64256593	2.09320891	2.86243862
$\psi = 0.01$	1.05355452	1.15839989	1.34047946	1.62113483	2.03902776
$\psi = 0.1$	0.45511518	0.47159449	0.49611975	0.52628508	0.55965313

extending the life period of the bearing system.

4. CONCLUSION

The graphical representation makes it clear that the adversarial influence of roughness can be remunerated up to a considerable extent by the affirmative influence of couple stress and magnetization in the case of negatively skewed roughness particularly when variance (-ve) occurs.

This article directs that the roughness features must be given attention while designing the bearing system even if an appropriate combination of magnetization parameter and couple stress parameter is in place.

Needless to say is that the positive effect of couple stress enriches by the ferrofluid lubrication. A distinct feature of this type of bearing system is that in spite of the presence of a half a dozen of parameters bringing down the load; the bearing supports some amount of load even in the lack of flow, which does not occur in the case of traditional lubricant based bearing system.

APPENDIX

In the nonexistence of body forces and body movements the equations of motion given by stokes (1966) are

$$\nabla \bar{v} = 0 \tag{A1}$$

$$\rho \frac{D\bar{v}}{Dt} = -\nabla p + \mu \nabla^2 \bar{v} - \eta \nabla^4 \bar{v} \tag{A2}$$

In view of the traditional assumption of hydrodynamic lubrication of thin film the above two equations take the following forms in the occurrence of a couple stress fluid.

$$\mu \frac{\partial^2 u}{\partial y^2} - \eta \frac{\partial^4 u}{\partial y^4} = \frac{\partial p}{\partial x} \tag{A3}$$

$$\mu \frac{\partial^2 w}{\partial y^2} - \eta \frac{\partial^4 w}{\partial y^4} = \frac{\partial p}{\partial z} \tag{A4}$$

$$\frac{\partial p}{\partial y} = 0 \tag{A5}$$

$$\frac{\partial u}{\partial x} + \frac{\partial v}{\partial y} + \frac{\partial w}{\partial z} = 0 \tag{A6}$$

The relevant boundary conditions are as in Biradar (2012). Let us remember that the flow of couple stress fluid in the porous matrix is described by

$$\bar{q}^* = \frac{-\phi}{\mu(1-\beta)} \nabla p^* \tag{A7}$$

where β represents the ratio of microstructure size to pore size. The pressure p^* in the porous region is governed by

$$\frac{\partial^2 p^*}{\partial x^2} + \frac{\partial^2 p^*}{\partial y^2} + \frac{\partial^2 p^*}{\partial z^2} = 0 \tag{A8}$$

ACKNOWLEDGEMENTS

The authors acknowledge the fruitful comments and suggestions of the reviewers/editors which has led to an enhancement in the presentation and organization of the article. Indeed, the appendix occurs exclusively due to the advice of one of the reviewers.

REFERENCES

Biradar, K. (2012). Squeeze film lubrication between parallel stepped plates with couple stress fluids. *International journal of Statistika and Mathematica* 3(2), 65-69.

Biradar, T. (2013). Squeeze film lubrication between porous parallel stepped plates with couple stress fluids. *Tribology online* 8(5), 278-284.

Bujurke, N. (1987). Rayleigh step bearing with second-order fluid. *Japanese Journal of Applied physics* 26(12), 2121-2126.

Christensen, H. and K. Tonder (1969a). Tribology of rough surface: Stochastic models of hydrodynamic lubrication. *SINTEF*, Report 10/69-18.

Christensen, H. and K. Tonder (1969b). Tribology of rough surfaces: parametric study and comparison of lubrication models. *SINTEF*, Report 22/69-18.

Christensen, H. and K. Tonder (1970). The hydrodynamic lubrication of rough bearing surfaces of finite width. *ASME-ASLE Lubrication conference*, Cincinnati, Ohio. Paper no. 70-Lub-7.

Deheri, G., H. Patel and R. Patel (2006). A study of magnetic fluid based squeeze film between infinitely long rectangular plates and effect of surface roughness, *International conference on Tribology*, Parma, Italy.

Elkouh, A. and D. Yang (1991). Flow of power-law fluid in a Rayleigh step. *Transactions of the ASME* 113, 428-433.

Guha, S. (2004). A theoretical analysis of dynamic characteristics of finite hydrodynamic journal bearings lubricated with coupled stress fluids. *Journal of Engineering Tribology* 218, 125-133.

Gupta, J. and G. Deheri (1996). Effect of roughness on the behavior of squeeze film in a spherical bearing. *Tribology Transactions* 39, 99-102.

Huang, W. and X. Wang (2016). Ferrofluids lubrication: a status report. *Lubrication Sciences* 28, 3-26.

Hughes, W. (1963). The magnetohydrodynamic finite step slider bearing. *Journal of Basic Engineering* 129-136.

Lin, J. (1998). Squeeze film characteristics of finite journal bearings: couple stress fluid model. *Tribology Int* 31 (4), 201-207.

Lin, J., C. Hung and R. Lu (2006). Averaged inertia principle for non-Newtonian squeeze films in wide parallel plates couple stress fluid model. *Journal of Marine Science and Technology* 14(4), 218-224.

Maiti, G. (1973). Composite and step slider bearings in micro polar fluids. *Japanese journal of applied physics* 12(7), 1058-1064.

Neuringer, J., R. Rosensweig (1964). Magnetic fluids. *Physics of fluids* 7(12), 1927-1937.

Patel, H., G. Deheri and R. Patel (2008). Performance of magnetic fluid based rotating rough circular step bearings. *International Journal of Applied Mechanics and Engineering* 13(2), 441-455.

Patel, H., G. Deheri and R. Patel (2008, January). Behavior of squeeze film between rough porous infinitely long parallel plates with porous matrix of variable thickness, *16th*

International colloquium Tribology, Germany, 15-17.

Patel, J. and G. Deheri (2016). Performance of a ferrofluid based rough parallel plate slider bearing: A comparison of three magnetic fluid flow models. *Advances in Tribology* 2016, ARTICLE ID 8197160, 9 pages.

Patel, N., D. Vakharia, G. Deheri and H. Patel (2017). Experimental performance analysis of ferrofluid based hydrodynamic journal bearing with different combination of materials. *Wear* 376-377, 1877-1884.

Prakash, J. and K. Tiwari (1983). Roughness effect in porous circular squeeze plates with arbitrary wall thickness. *Journal of Lubrication Technology* 105, 90-95.

Ramanaiah, G. and J. Dubey (1975). Micropolar fluid lubricated squeeze films and thrust bearings. *Wear* 32(3), 343-351.

Ramanaiah, G. and P. Sarkar (1978). Squeeze films and thrust bearings lubricated by fluids with couple stress. *Wear* 48(2), 309-316.

Scherer, C. and A. Figueiredo Neto (2005). Ferrofluids: Properties and applications. *Brazilian Journal of Physics* 35(3A), 718-727.

Shimpi, M. and G. Deheri (2012). Magnetic fluid based squeeze film performance in rotating curved porous circular plates: The effect of deformation and surface roughness. *Tribology in Industry* 34(2), 57-67.

Siddangouda, A. (2015). Combined effects of surface roughness and non-Newtonian couple stresses squeeze film characteristics between parallel stepped plates. *International Journal of Mathematical* 6(2), 113-121.

Stokes, V. (1966). Couple stresses in fluids. *The Physics of fluids* 9, 1709-1715.

Vadher, P., V. Pothodichackaru, G. Deheri and R. Patel (2008). Behaviour of hydromagnetic squeeze films between two conducting rough porous circular plates, *Journal Engineering Tribology, Proc. IMechE,* 222, 569-579.